ACTA ASTRONOMICA
Vol. **80** (2022) pp. 0–0

New photometric and spectroscopic observations of the eclipsing binary V2080 Cygni[1]

W. Dimitrov[1], K. Kamiński[1], K. Bąkowska[2],
M. K. Kamińska[1], J. Tokarek[1], M. Pawłowski[1], D. Boneva[3],
P. Bartczak[1] T. Kwiatkowski[1], A. Schwarzenberg–Czerny[4]

[1] Astronomical Observatory Institute, Faculty of Physics,
Adam Mickiewicz University, ul. Słoneczna 36, 60-286 Poznań, Poland
e-mail: dimitrov@amu.edu.pl
[2] Institute of Astronomy, Faculty of Physics, Astronomy and Informatics,
Nicolaus Copernicus University, ul. Grudziądzka 5, 87-100 Toruń, Poland
[3] Space Research and Technology Institute, Bulgarian Academy of Sciences,
Acad. Georgi Bonchev St., Sofia 1113, Bulgaria
[4] Nicolaus Copernicus Astronomical Center, ul. Bartycka 18, 00-716 Warsaw, Poland

Received January 30, 2021

ABSTRACT

We present new spectroscopic and photometric measurements of the eclipsing binary V2080 Cygni. It is a detached system with similar components and an orbital period of 4.9 d. We collected spectroscopic data with two instruments, 1.88 m DDO telescope equipped with Cassegrain spectrograph and 0.5 m PST1 connected to a fiber-fed echellé spectrograph. We collected 127 measurements for each component, which significantly increase the number of available radial velocity measurements for the V2080 Cygni system. Obtained masses of the eclipsing components are $M_1 = 1.189 \pm 0.007$ M$_\odot$ and $M_2 = 1.138 \pm 0.007$ M$_\odot$. We also collected a multicolor photometry. The three-band light curves obtained together with the radial velocity data enabled us to calculate the model of the system. New estimations of the orbital inclination and radii of the components were computed. We obtained as well new times of minima. The $O-C$ diagrams indicate variation, which requires more recent data to be confirmed. The possible existence of a third body could cause a light-time effect in the system. In addition, we analyze the GAIA mission results. V2080 Cygni A has three visual companions; however, according to GAIA parallaxes and proper motions, they cannot be dynamically connected with the eclipsing binary and therefore are background stars.

Key words: *Stars: individual: V2080 Cygni - binaries: eclipsing*

1. Introduction

Detached eclipsing binaries provide a precise determination of stellar radii and masses. Modern photometric and spectroscopic observations allow us to reach an

[1] Based on the spectroscopic data obtained with Poznań Spectroscopic Telescope 1 and David Dunlap Observatory 1.88 m telescope.

accuracy of about 1% or better for these absolute parameters. The investigated star V2080 Cygni is an F5 type eclipsing binary (EB) with a visual magnitude of 7.4. Other designations of the object are HD 183361 and BD+49 3012. The binary is listed as a visually multiple star in Catalog of the Components of Double and Multiple Stars (CCDM; Dommagnet & Nys 1994) and Washington Double Star Catalog (WDS; Mason et al. 2001). The eclipsing nature of the main A star was detected by the Hipparcos satellite mission. The light curve (LC) has flat maxima and minima with comparable depth, as can be expected for similar, almost spherical components. The object is relatively bright and close, i.e. it is a good candidate for precise determination of absolute parameters. Spectral lines of both V2080 Cygni components are clearly seen. First radial velocity (RV) measurements were presented in a short IBVS paper (Kurpinska-Winiarska et al. 2000). The authors provided the amplitudes of the radial velocity curves. They corrected the orbital period of the star, which is twice as long as the one given by Hipparcos. Later on, two teams observed the star spectroscopically. The first group collected 13 spectra at the TUBITAK National Observatory and Catania Astrophysical Observatory (İbanoğlu et al. 2008). The velocities were measured with the cross-correlation method. The authors also observed the star photometrically and acquired UBV light curves. They obtained a model of the system using the Wilson-Devinney method. The authors mentioned the existence of the third light in the system of about 3%. The second team used 8 spectra obtained with the ELODIE spectrograph (Aliçavuş et al. 2019). For the analysis, they used the spectral disentangling method. Atmospheric parameters were obtained as well. For the modeling of the star, authors also used previously obtained radial velocity measurements of the first team and the SuperWASP light curve. The authors detected a third light of about 8% in both light curve modeling and spectrum disentangling. The results for masses from both studies agree within errors. The mass ratio is close to 1 and the obtained masses are 1.197 ± 0.005 $M_\odot$ for the primary component and 1.173 ± 0.004 $M_\odot$ for the secondary.

2. Visual companions

As mentioned in the Introduction, V2080 Cyg A has three bright visual companions. They are listed in the WDS and CCDM catalogs of visual doubles. The latest results coming from GAIA mission[2] yield the parallaxes and proper motions of all four components (Gaia Collaboration et al. 2016; Lindgren et al. 2016). GAIA DR2 results are presented in Table 1. Both DR1 and DR2 results are in good agreement and show that all the components have different parallaxes and proper motions and are not connected dynamically. The fainter stars in the close neighborhood also seem to be background stars, their proper motions and parallaxes are small (Fig. 1).

[2]https://gea.esac.esa.int/archive/

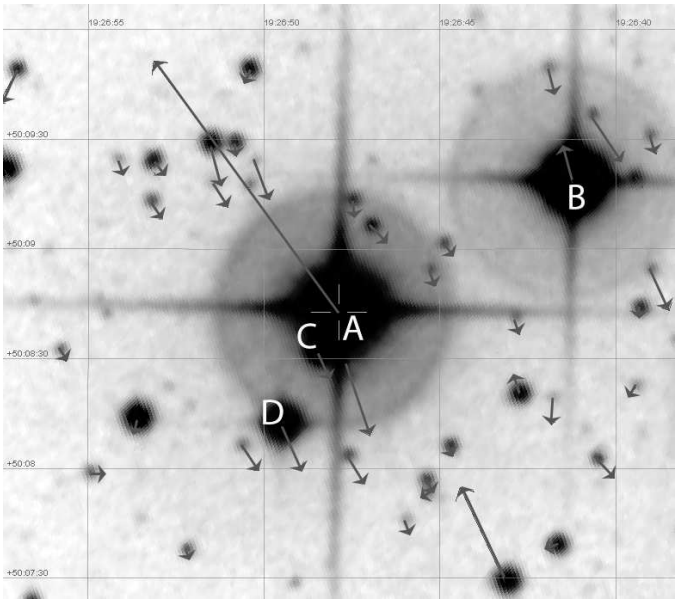

Fig. 1. Proper motions of V2080 Cyg A neighborhood stars (GAIA DR2).

T a b l e 1

Proper motions and parallax for V2080 Cyg A and its potential companions from the GAIA DR2 catalog.

comp. WDS	phot. g (mag)	sep. (arcsec)	μ_α (mas/yr)	μ_δ (mas/yr)	parallax (mas)
A	7.24	-	55.50 ± 0.07	75.01 ± 0.07	11.70 ± 0.03
C	14.08	14	-2.97 ± 0.04	-5.94 ± 0.04	0.48 ± 0.03
D	11.49	36	-6.21 ± 0.06	-13.51 ± 0.05	0.57 ± 0.03
B	8.57	73	2.36 ± 0.13	10.41 ± 0.11	2.55 ± 0.05

3. Spectroscopic observations and RV measurements

Each of the two spectroscopic data sets used in the present study has been obtained with a different instrument. In the first approach, they were both independently analyzed and compared with each other, as well as with data from the literature. Our spectroscopic observations complement existing data and increase the number of all available observations by about four times.

The first data set was obtained with the 1.88 m telescope of David Dunlap Observatory with the Cassegrain spectrograph between April 21^{st} and November 10^{th} 2006. Two different detectors were used: 1024x1024 Thomson CCD and,

V

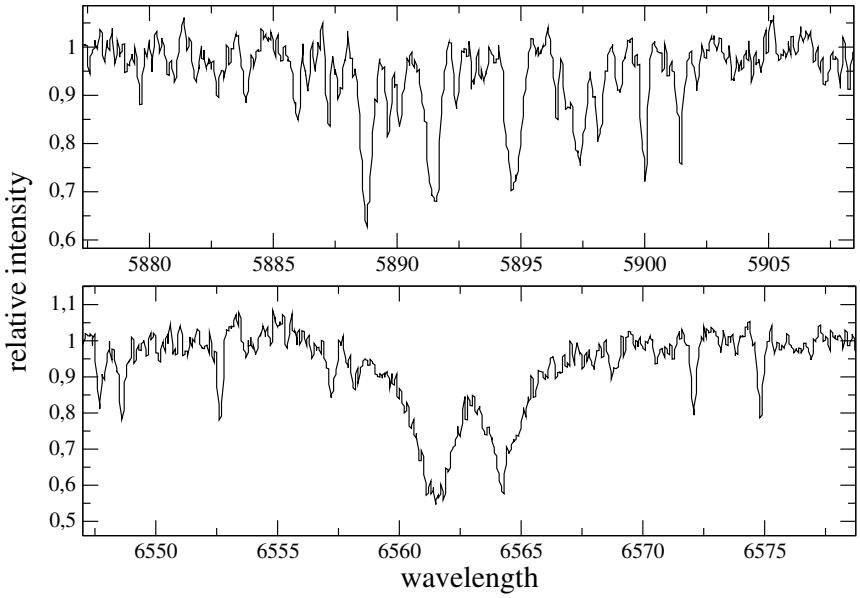

Fig. 2. Two spectral regions of a PST 1 spectrum: near NaD (top) and H_α (bottom) lines.

later, 2048x512 Jobin Yvon Horiba CCD. The exposure times were 1200 s and we observed the Mg spectral region near 5184 Å. The typical signal–to–noise ratio was in the range of 100 – 150. Data reduction was carried out using standard IRAF tasks.

The second dataset was acquired with a 0.5 m Poznan Spectroscopic Telescope (PST1) between June 16^{th} and October 14^{th} 2007. This instrument is smaller than the previous one; however, it is connected via fiber to an echellé spectrograph (Baranowski et al. 2009). The system has very small light losses, as the telescope parameters fit perfectly the fiber requirements. The spectrograph is equipped with Andor DZ 436 CCD with 5 stage peltier plus liquid cooling. The spectral range was 4500 – 9200 Å with dispersion of 0.11 Å/pix. The exposure times were 1200 or 1800 s and the typical signal–to–noise ratio is 25 – 125. Two spectral regions are presented in Fig. 2. The split spectral lines of both components are clearly seen.

We searched for traces of the third star, mentioned by the previous authors, in the cross-correlation function. To enhance the signature of this component we used low-temperature templates. We have not found any significant traces (Fig. 3).

For radial velocity measurements, we have used the Broadening Function[3] (BF) method, and for comparison and tests we also used the Cross-Correlation (CCF) method. The Broadening Function was first described by S. Rucinski (1992, 2002). The method is resistant to spectral line broadening and has higher resolution compared to that of CCF. Typical BF for V2080 Cygni spectra is presented in Figure

[3]http://www.astro.utoronto.ca/ rucinski/SVDcookbook.html

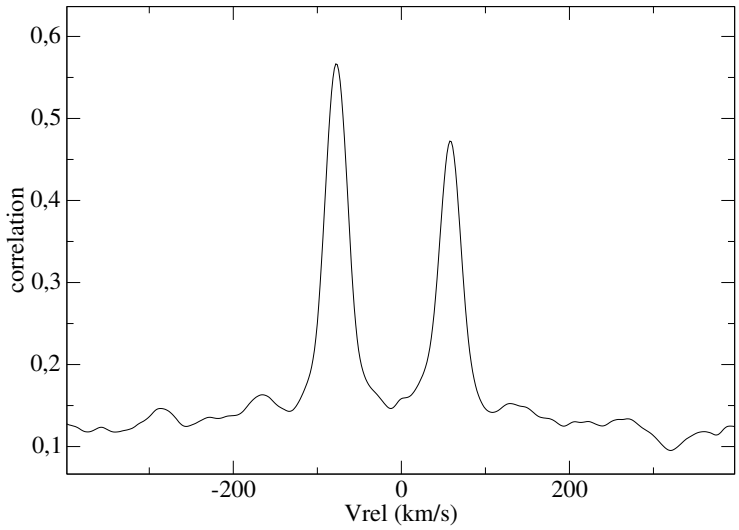

Fig. 3. Example of cross correlation function obtained for PST 1 spectrum, which was used during the search for third light in the system.

4. The two peaks of similar height are well resolved. A simple sine fit reveals the amplitudes of the RV curves: $K_1 = 80.8$ km s^{-1} and $K_2 = 84.4$ km s^{-1}. The corresponding mass ratio is 0.957. The cross-correlation measurements were carried out with IRAF task FXCOR.

4. Photometry and times of minima

4.1. Observations and data reduction

Observations of V2080 Cyg were obtained during 41 nights between September 7^{th} to October 1^{st} 2011 at the Poznań Astronomical Observatory located in Poland. For observations we used a 200 mm, F/4.5 Newton reflector, equipped with SBIG ST-7 XME camera and a set of Bessel BVRI filters. The camera provided $17.0' \times 25.5'$ field of view. All observations were carried out in the V, I, and R filters with exposure times of 10, 8, and 6 seconds, respectively. In total, we obtained 50699 exposures of V2080 Cyg during 108.59 hours. Table 2 presents a full journal of our CCD observations.

We determined the relative unfiltered magnitudes of V2080 Cyg by taking the difference between the magnitude of the object and the mean magnitude of three comparison stars. In Fig. 5 the sky region is displayed with V2080 Cygni marked as V1 and the comparison stars as C1, C2, and C3, respectively. The equato-

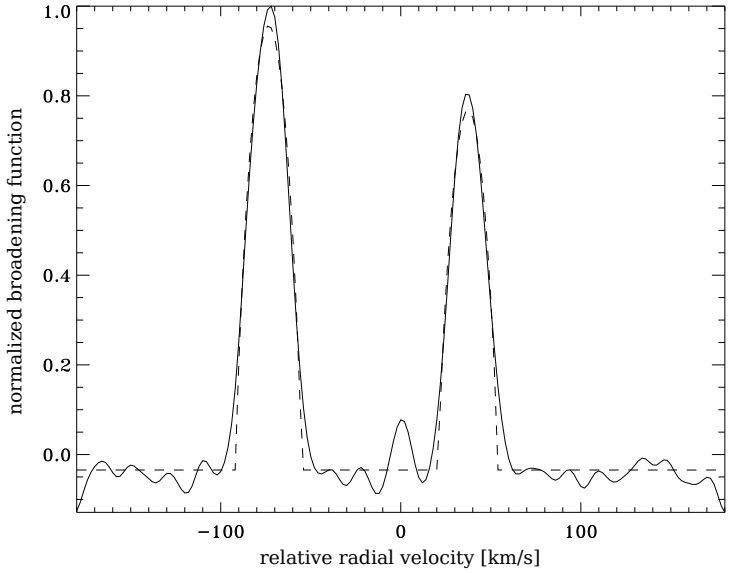

Fig. 4. Broadening function for one of the PST1 spectra. Solid line represents the BF and dashed line the fitted rotational profiles. The BF is normalized to 1. The horizontal axis represents the relative radial velocity. The third peak, near 0, is related to the telluric lines.

rial coordinates and brightness of the comparison stars C1 (RA$= 19^h26^m41^s.246$, Dec$= +50^o09'18".274$, 8.56 mag in the V filter), C2 (RA$=19^h27^m00^s.870$, Dec$=+50^o14'04".884$, 8.98 mag in the V filter), and C3 (RA$=19^h27^m16^s.991$, Dec$=+50^o16'10".986$, 10.08 mag in the V filter) were taken from the Tycho-2 Catalog (Høg et al. 2000).

CCD frames were reduced with the *STARLINK*[4] package (Currie 2014). Corrections for bias, dark current, and flat-field were applied, and the aperture photometry was conducted. In Fig. 8 (Sect. 5) we present the resulting light curves of V2080 Cygni in I, R, and V filters.

4.2. $O-C$ diagram for eclipses

To check the stability of the orbital period and determine its value, the $O-C$ analysis was carried out. First, we used the timings of five eclipses from our 2009-2011 observing season, and the following ephemeris of the minima was derived:

$$\mathrm{HJD}_{\mathrm{min}} = 2455094.3114(2) + 4.933550(2) \times E, \qquad (1)$$

which gives the orbital period of $P_{orb1} = 4.933550(2)$ days.

To obtain the best possible value of the orbital period we combined our five timings of eclipses from September 2009 - September 2011 observations, the Su-

[4]The Starlink software is currently supported by the East Asian Observatory

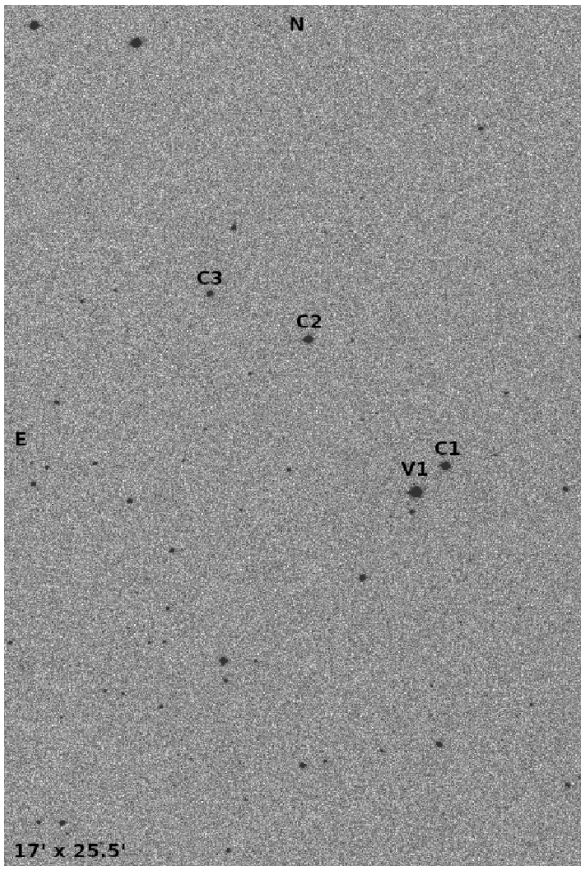

Fig. 5. Finding chart of V2080 Cyg. The variable is marked as V1. Positions of the three comparison stars C1, C2, and C3 are also shown. The field of view is about 17.0' $\times$ 25.5'. North is up, east is to the left.

Table 2: The journal of the CCD observations of V2080 Cyg.

Year	Start date	End date	Number of nights	Exposure time [sec]	Number of frames	Filter
2009	September 7	November 21	19	10	6306	V
				8	7248	I
				6	9550	R
2010	October 17	October 31	5	10	1726	V
				8	2141	I
				6	3012	R
2011	May 23	October 1	17	10	5515	V
				8	6888	I
				6	8313	R
Total:	-	-	41	-	50699	-

perWASP[5] June-July 2008 data set, and the date presented in İbanoğlu et al. (2008). Based on this, we calculated the following ephemeris of the minima:

$$\mathrm{HJD}_{\mathrm{min}} = 2455094.31027(9) + 4.9335701(4) \times E, \quad (2)$$

and this corresponds to the orbital period of $P_{orb2} = 4.933701(4)$ days. In Fig. 6 we show the resulting $O-C$ diagram for the moments of eclipses for the 1998-2011 time span. In Table 3 we present the timings of eclipses with errors, cycle numbers E and $O-C$ values. The primary and secondary eclipses observed in V2080 Cyg are marked as Type I and Type II, respectively. The decreasing trend of the orbital period shown in Fig. 6 was confirmed by calculations of the second-order polynomial fit to the moments of minima. The following ephemeris was obtained:

$$\mathrm{HJD}_{\mathrm{min}} = 2455094.31054(9) + 4.9335634(6) \times E - 2.7(2) \times 10^{-8} \times E^2. \quad (3)$$

In Fig. 6 the solid line corresponds to the ephemeris given by Eq. 3.

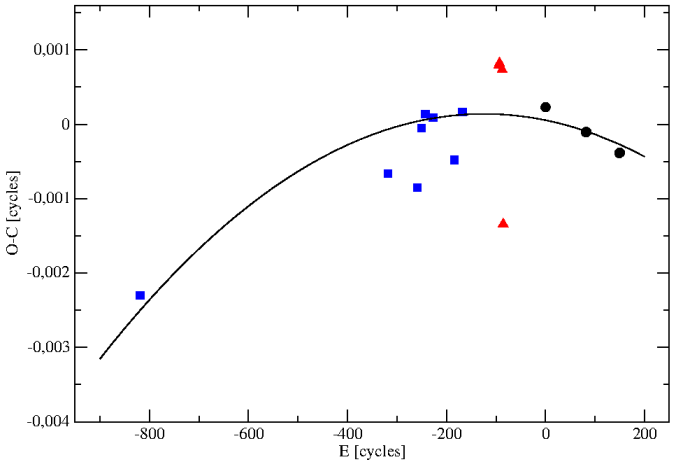

Fig. 6. The $O-C$ diagram of the moments of eclipses in V2080 Cyg based on data collected between 1998 and 2011 from both literature and our measurements. Black circles represent our dataset, data taken from the SuperWASP is marked with red triangles, and blue squares correspond to data provided by İbanoğlu et al. (2008).

After this investigation, we suggest that the orbital period might have not been stable between August 1998 and September 2011 and can be described by a decreasing trend with a rate of $\dot{P} = -2.7(2) \times 10^{-8}$. It should be noted that the

[5]https://wasp.cerit-sc.cz

observed change in the orbital period, presented in Fig. 6, was calculated based on the only one point of data from 1998 given by İbanoğlu et al. (2008). Hence, this time span of observations and the amount of available data are insufficient for any conclusive statement pertaining to the changes in the orbital period of V2080 Cygni.

In the observed curves, one can see an unusual feature around phase 0.18. It is almost invisible in the V filter, shows a brightness decrease in the R filter, and has a hump shape in infrared. We suspect that this feature is an artifact (due to the lower quality of the data) rather than any physical process manifestation in V2080 Cyg. In particular, we often gathered outside minima data in unfavorable weather conditions, and consequently, parts of the datasets are more scattered than others.

Table 3: Times of minima in the light curves of V2080 Cyg observed since August 1998 until September 2011.

E	$\mathrm{HJD}_{\mathrm{min}} - 2450000$	Error	$O-C$ [cycles]	Type	Reference
-819	1053.7050	-	-0.00230221	II	İbanoğlu et al. (2008)
-318	3525.4317	0.0008	-0.00066447	II	İbanoğlu et al. (2008)
-259	3816.5114	0.0006	-0.00085417	II	İbanoğlu et al. (2008)
-250.5	3858.4507	0.0003	-0.00005269	I	İbanoğlu et al. (2008)
-243	3895.4534	0.0001	0.00013467	II	İbanoğlu et al. (2008)
-227	3974.3903	0.0006	0.00089732	II	İbanoğlu et al. (2008)
-184	4186.5310	0.0003	-0.00048071	II	İbanoğlu et al. (2008)
-168	4265.4713	0.0006	0.00016353	II	İbanoğlu et al. (2008)
-94	4630.5586	0.0005	0.00079444	II	SuperWASP
-93	4635.4923	0.0008	0.00082077	II	SuperWASP
-87.5	4662.6265	0.0005	0.00073248	I	SuperWASP
-85.5	4672.4834	0.0006	-0.00134313	I	SuperWASP
0	5094.3114	0.0002	0.00022904	II	This work
81.5	5496.3957	0.0002	-0.00010807	I	This work
82.5	5501.3293	0.0003	-0.00010201	I	This work
149	5829.4103	0.0003	-0.00038814	II	This work
150	5834.3439	0.0004	-0.00038208	II	This work

5. Model of the system

For fitting of the radial velocity and photometric curves we have employed the PHOEBE SVN code (Prša & Zwitter 2005). The program is based on the Wilson-

Devinney method (Wilson & Devinney 1971). As the results of the previous investigations suggest that the eclipsing pair could have a companion, we fitted the two RV data sets separately to check for shifts between them. We found a difference between the systemic velocities for both data sets of 1.1 $km\ s^{-1}$. For the simultaneous fit, we shifted up the first data set (DDO) by this value. For the analysis, we adopted period value of $P_{orb2} = 4.9335701(4)$ days (eq. 2) based on the times of minima collected by different authors.

For the determination of the temperatures, we used the color temperature of the system $6255 \pm$K based on the color index $J-H = 0.257$. In the first approximation we fixed the temperature of the main component T_1 to this value and fitted the T_2. Next, we adjusted the temperatures of both components to be in agreement with the system color temperature. For this purpose, we used the formulas given by Kjurkchieva and Vasileva (2015). For modeling, we used a logarithmic limb darkening law and Van Hamme (1993) coefficients. Both components have convective envelopes so we used albedo coefficients of 0.5 and gravity darkening coefficients of 0.32. The search for third body signature in our spectroscopy did not yield positive results and the fitted value of the third light was negligible – very close to zero. Consequently, we fixed the value of l_3 to zero.

Both stars are almost spherical, R_{point} and R_{side} for both components differ by less than 1%. The differences between the results of radial velocity fitting for the point source and the full model are very small, below the error bars. For example, the size of the semi-major axis differs by 0.01%. For our final solution we used the full model, which also presents the Rossiter effect on the RV curve. We assumed a synchronous rotation for both components and a circular orbit.

Figures 7 and 8 present our best fit. In Table 4 we compare our results with those from previous publications of Aliçavuş et al. (2019), İbanoğlu et al. (2008) and Kurpińska-Winiarska et al. (2000). Most of the results are comparable or differ slightly above the error bars. The systemic velocity differs significantly, which could be caused by a potential third body in the system. In case of the absolute parameters, our mass estimation for the secondary component is the lowest among the results. İbanoğlu et al. (2008) present a noticeably different result for the radii with almost equal values for both components. The investigations used different photometric bands. For comparison of the luminosities we used the visual band as it was the only common band. In case of SWASP data used by Aliçavuş et al. (2019), the band is broader, but the central wavelength is very close to the one of V filter.

We performed one of the bootstrap method variants to verify our error estimations. We randomly drew N measurements from N observations with possible repetitions of values, where N is the number of observations in a given LC or RV data set. In this way we obtained ten sets of data and fitted radial velocity and light curves to each of them. We calculated the standard deviation of obtained values of the parameters. Our formal errors from the program are comparable or in some

T a b l e 4

Comparison of V2080 Cygni parameters obtained in this work with values from the literature.

	Kurpińska-Winiarska et al. 2000	İbanoğlu et al. 2008	K. Aliçavuş & Aliçavuş 2019	PST1 & DDO (this paper)
i		$86.^{\circ}20 \pm 0.10$	$86.^{\circ}009 \pm 0.091$	$86.^{\circ}03 \pm 0.02$
q	0.974	0.971 ± 0.009	0.982 ± 0.002	0.957 ± 0.002
a ($R_{\odot}$)		16.20 ± 0.07	16.254 ± 0.019	16.155 ± 0.026
V_{γ} (km s^{-1})	3.2	1.0 ± 0.4	1.17 ± 0.32	2.88 ± 0.08
T_1(K)		6000 ± 75	6100 ± 100	6270 ± 40
T_2(K)		5987 ± 75	6210 ± 250	6240 ± 40
Ω_1		11.132 ± 0.002	10.339 ± 0.179	10.706 ± 0.029
Ω_2		10.862 ± 0.002	11.925 ± 0.242	10.846 ± 0.053
$L_1/(L_1+L_2)$ (V)		0.501 ± 0.002	0.568 ± 0.024	0.530 ± 0.003
$L_2/(L_1+L_2)$ (V)			0.432 ± 0.020	0.470 ± 0.005
l_3 (V)		0.029 ± 0.003	0.083 ± 0.015	0
M_1 ($M_{\odot}$)		1.191 ± 0.017	1.197 ± 0.005	1.189 ± 0.007
M_2 ($M_{\odot}$)		1.157 ± 0.017	1.173 ± 0.004	1.138 ± 0.007
R_1 ($M_{\odot}$)		1.596 ± 0.008	1.734 ± 0.031	1.659 ± 0.005
R_2 ($M_{\odot}$)		1.599 ± 0.008	1.459 ± 0.029	1.575 ± 0.009
n_{obs}(RV)	11	13	21	127
method	-	CCF	CCF	BF

cases 2 – 3 times lower than the bootstrap errors listed in the last column of Table 4.

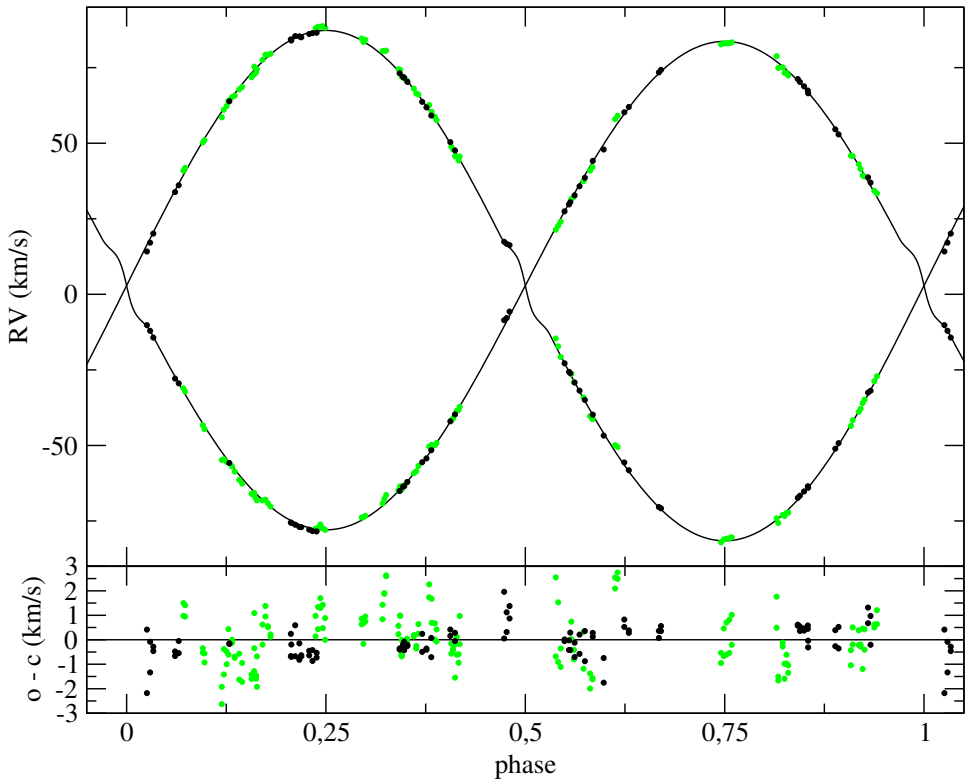

Fig. 7. Radial velocity curves of V2080 Cygni. Green dots represent DDO measurements shifted up by 1.1 $km\ s^{-1}$. Black dots represent measured PST1 velocities while the straight lines – synthetic RV curves based on the model listed in the last column of Table 4.

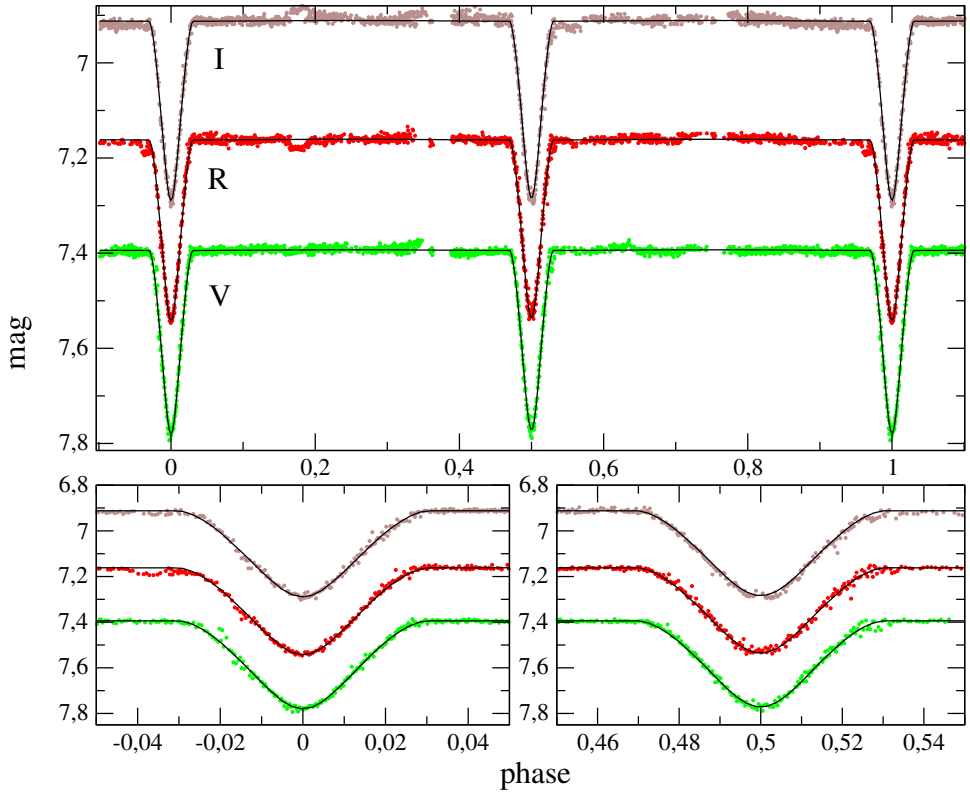

Fig. 8. The results of our V2080 Cygni multicolor photometry compared with the synthetic light curves. Lower panels present zoomed primary and secondary minima.

6. Conclusions

V2080 Cygni, the object of the study, is located in a dense field of stars. The binary has three visual companions; however, the GAIA proper motion and parallax results reveal that they are not connected with the EB as well as the dimmer background stars. There are clues that there is a third body in the system. We did not find traces of third light in our spectra, however, Aliçavuş et al. (2019), using the spectral disentangling method and spectra with slightly higher signal–to–noise ratio and resolving power, found 8% light contribution of the third component. Such a luminosity corresponds to a main-sequence star with a mass of about 0.9 $M_{\odot}$. Moreover, during the light curve analysis the authors fitted the l_3 value; nevertheless, we know that there is a strong correlation between the third light and the mass ratio or orbital inclination. Additionally, the times of minima shows some shifts with respect to the ephemeris. The analysis of eclipse times show possible variation of the orbital period, which must be confirmed with new measurements. Those variations could be related to a third body and the light-time effect in the system. However, due to the fact that some of the arguments are contradictory and some measurements are insufficient, we cannot conclude the existence of a third body in the system.

We analyzed our two radial velocity data sets obtaining a new mass determination (for both EB components) based on a significantly higher number of measurements than the previous investigations. Comparing our data with those of the literature, we found, as we can expect, that the results depend on the usage of different instruments and different measurement methods. We estimated the effect of systematic errors on the resulting measurements of masses to be about 1–2%, while our bootstrap errors of the model equal 0.6%.

We could compare our two datasets obtained on the 1.88 m DDO telescope and the 0.5 m PST1 telescope. The signal-to-noise ratio of the DDO spectra is higher; however, the PST1 echellé has a wider spectral range. The dispersion of the RV measurements for PST1 is smaller as can be expected for the spectrograph mounted in a thermally stabilized room. The measured semi-major axis of V2080 Cygni is in very good agreement, but the mass ratio differs by about 1%, which propagates into 1% differences in masses.

A comparison of our result with the previous investigations shows that our primary mass value is close to the one obtained by İbanoğlu et al. (2008), while the secondary is about 2% lower. Masses obtained by Aliçavuş et al. (2019) are the highest among all results. Our model yields the lowest value of the mass ratio of the eclipsing pair.

Acknowledgements. We would like to thank Slavek M. Rucinski and DDO staff for generous hospitality. In particular, our team wants to express appreciation to the observers Heide DeBond and Jim Thomson. The authors are grateful to our

engineer Roman Baranowski, co-founder of the Poznań Spectroscopic Telescope project. We also wish to thank the people who helped in the observations: Agata Rożek, Krystian Kurzawa, Anna Przybyszewska and Adrian Kruszewski. WD, TK, KK and ASC were supported by the Polish grant KBN 1 P03D 025 29.

This work has made use of data from the European Space Agency (ESA) mission *Gaia* (http://www.cosmos.esa.int/gaia), processed by the *Gaia* Data Processing and Analysis Consortium (http://www.cosmos.esa.int/web/gaia/dpac/consortium, DPAC). Funding for the DPAC has been provided by national institutions, in particular the institutions participating in the *Gaia* Multilateral Agreement.

REFERENCES

Baranowski, R., Smolec, R., Dimitrov, W. et al. 2009, *MNRAS*, **396**, 4.
Currie, M. J., Berry, D. S., Jenness, T. et al. 2014, *ASPC*, **485**, 391C.
Dommanget, J. and Nys, O. 1994, *Communications de l'Observatoire Royal de Belgique*, **115**, 1.
Gaia Collaboration Brown, A. G. A. et al. 2016, *A&A*, **595**, 2.
Høg, E. et al. 2000, *A&A*, **355L**, 27H.
İbanoğlu, C. et al. 2008, *MNRAS*, **384**, 1.
Kahraman Aliçavuş, F. and Aliçavuş, F. 2019, *MNRAS*, **488**, 4.
Kjurkchieva, D. and Vasileva, D. 2015, *Bulg. Astron. J.*, **23**, 75K.
Kurpińska-Winiarska, M., Oblak, E., Winiarski, M. and Kundera, T. 2000, *IBVS*, **4823**, 1-3.
Lindegren, L. et al. 2016, *A&A*, **595**, 4.
Mason, B. D., Wycoff, G. L., Hartkopf, W. I., Douglass, G. G. and Worley, C. E. 2001, *AJ*, **122**, 3466.
Prša, A. and Zwitter, T. 2005, *ApJ*, **628**, 426.
Slavek Rucinski 1992, *AJ*, **104**, 1968R.
Slavek Rucinski 2002, *AJ*, **124**, 1746R.
Van Hamme, W. 1993, *AJ*, **106**, 2096.
Wilson, R. E. and Devinney, E. J. 1971, *ApJ*, **166**, 605.